The green tea catechin EGCG provides proof-of-concept for a pan-coronavirus entry inhibitor

Emmanuelle V. LeBlanc[1] and Che C. Colpitts[1,#]

[1]Department of Biomedical and Molecular Sciences, Queen's University, Kingston, ON K7L 3N6, Canada

[#]Correspondence: che.colpitts@queensu.ca

Abstract

The COVID-19 pandemic caused by the severe acute respiratory syndrome coronavirus-2 (SARS-CoV-2) has emphasized the serious threat to human health posed by emerging coronaviruses. Effective antiviral countermeasures are urgently needed as vaccine development against an emerging coronavirus takes time, even in the best-case scenario. The green tea catechin, epigallocatechin gallate (EGCG), has broad spectrum antiviral activity. We demonstrate here that EGCG prevents murine and human coronavirus infection and blocks the entry of lentiviral particles pseudotyped with spike proteins from bat or highly pathogenic coronaviruses. We show that EGCG treatment reduces coronavirus attachment to target cell surfaces. Our results demonstrate the potential for the development of pan-coronavirus attachment inhibitors.

Key words

SARS-CoV-2, coronavirus, entry inhibitor, natural product

24 **Introduction**

25 The novel severe acute respiratory syndrome coronavirus-2 (SARS-CoV-2) has infected hundreds
26 of millions of people and has resulted in millions of deaths around the world. The COVID-19
27 pandemic, caused by SARS-CoV-2, underscores the severe health threat posed by emerging
28 coronaviruses (CoVs), and makes evident the paucity of antivirals with extended spectrums of
29 activity. SARS-CoV-2 is the third highly pathogenic CoV to emerge in the 21st century. The
30 abundance and diversity of SARS-related CoVs in bats points to the likelihood of future spillover
31 into human populations [1]. In addition, seasonally circulating common cold CoVs continually
32 burden human health [2], and cause severe disease in elderly populations [3,4], without effective
33 preventative or therapeutic strategies. In order to develop inhibitors that are effective against such
34 a broad range of endemic, pandemic, and emerging CoVs, a conserved step of viral infection needs
35 to be targeted.

36 Most human viruses, including CoVs, initiate primary attachment to cell surfaces through
37 low-affinity but high-avidity interactions with glycans. Heparan sulfate proteoglycans are
38 necessary attachment receptors for the human alphacoronavirus NL63 (HCoV-NL63) [5], as well
39 as many other human viruses, such as herpes simplex virus (HSV) [6,7], hepatitis C virus (HCV)
40 [8,9] and human immunodeficiency virus (HIV) [10]. Recently, heparan sulfate has also been
41 identified as a necessary co-factor for SARS-CoV-2 infection [11,12]. Alternatively, other viruses,
42 including influenza A virus (IAV) and betacoronaviruses HCoV-OC43 and HCoV-HKU1 require
43 sialic acid-containing glycans for attachment and entry [13–15]. Regardless of the glycan subtype,
44 glycan binding is critical to the primary attachment of many different viruses, facilitating their
45 specific high-affinity interaction with less abundant protein receptors, such as ACE2 for HCoV-

46 NL63, SARS-CoV-1 and SARS-CoV-2 [16,17]. For some viruses, like IAV, glycans serve as the
47 only known entry receptor.

48 Blocking viral attachment to cellular glycans is a demonstrated approach to inhibit diverse
49 viral infections. Epigallocatechin gallate (EGCG) is the most bioactive polyphenolic compound
50 from green tea with antiviral activity against diverse DNA and RNA viruses, including HSV-1,
51 HCV, and IAV [18]. The broad antiviral spectrum of EGCG has been attributed to its ability to
52 inhibit the primary attachment of unrelated viruses by competing with both heparan sulfate and
53 sialic acid for virion binding [19]. However, whether EGCG inhibits coronavirus infection by
54 similar mechanisms remains unknown.

55 Here, we show that EGCG inhibits infectivity of murine, bat, and human CoVs. Cell
56 surface binding of multiple human CoVs is blocked by EGCG, suggesting that this natural product
57 inhibits a conserved step in CoV attachment, such as initial binding to glycans. These findings
58 demonstrate that blocking primary attachment is a potential antiviral strategy to prevent infection
59 by diverse CoVs.

60

61 **Material and Methods**

62 **Compounds**

63 Epigallocatechin-3-gallate (EGCG) was purchased from Thermo Fisher Scientific (CAS 989-51-
64 5). Heparin was obtained from Carbosynth Ltd (YH09354).

65

66 **Plasmids**

67 Lentiviral pseudoparticles were produced using plasmids encoding HIV-1 gag/pol (BEI Resources
68 NR-52517), tat (BEI Resources NR-52518), rev (BEI Resources NR-52519), a luciferase-

69 encoding lentiviral genome (BEI Resources NR-52516) and spike plasmids. The SARS-CoV-2
70 spike expression plasmid was obtained from Dr. Raffaele De Francesco (Addgene plasmid #
71 155297). The MERS-CoV spike expression plasmid was kindly provided by Dr. Stefan Pöhlmann
72 (Göttingen, Germany). The SARS-CoV-1 (Tor2 strain, GenBank accession no. **NC_004718.3**) and
73 WIV1-CoV spike (GenBank accession no. **KC881007.1**) expression plasmids were synthesized
74 by Genscript and codon-optimized for human expression. The lentiviral vector expressing human
75 ACE2 was obtained from Dr. Sonja Best (Addgene plasmid # 154981).
76
77 **Cells and viruses**
78 HEK293T/17 (ATCC ACS-4500), L929 (ATCC CCL-1), Huh7 (JCRB0403), HCT-8 (ATCC
79 CCL-244), 17Cl-1 (BEI Resources NR-53719) and Vero E6 (ATCC CRL-1586) cells were
80 cultured in Dulbecco's minimal essential medium (DMEM) with 10% FBS, 50 U/mL penicillin,
81 and 50 µg/mL streptomycin at 37°C in 5% CO_2. A549 (BEI Resources NR-52268) cells were
82 cultured in Hams F-12K (Kaighn's) medium with 10% FBS, 50 U/mL penicillin, and 50 µg/mL
83 streptomycin, and 10 µg/mL blasticidin (for A549-ACE2 cells) at 37°C in 5% CO_2. Calu-3 (ATCC
84 HTB-55) cells were cultured in minimal essential medium (MEM) with 10% FBS, 1 mM sodium
85 pyruvate, 1X non-essential amino acid solution, 50 U/mL penicillin, and 50 µg/mL streptomycin
86 at 37°C in 5% CO_2.
87 Human coronavirus 229E (HCoV-229E) and HCoV-OC43 were obtained from BEI
88 Resources (NR-52726 and NR-52725). For HCoV-229E, Huh7 cells were infected with a
89 multiplicity of infection (MOI) of 0.01 plaque-forming units (pfu)/cell and incubated at 33°C in
90 5% CO_2 until full cytopathic effects (CPE) were observed (~5 days post-infection). The
91 supernatants were collected, and cellular debris was pelleted by centrifugation at 1,000 × g for 10

92 min. The resulting supernatant was then aliquoted, and the viral stocks were stored at −80°C. For
93 HCoV-OC43, HCT-8 cells were infected (MOI of 0.01) and incubated at 33°C in 5% CO_2 until
94 full CPE were observed (∼5 days post-infection). Similarly, supernatants were collected, cellular
95 debris was pelleted by centrifugation at 1,000 × g for 10 min and the resulting supernatant was
96 then aliquoted and stored at −80°C.

97 Green fluorescent protein-expressing murine hepatitis virus (MHV A59-GFP) was kindly
98 provided by Dr. Volker Thiel (Institute of Virology and Immunology, Bern, Switzerland) [20].
99 VSV-SARS-CoV-2 S was a gift from Dr. Sean Whelan (Washington University School of
100 Medicine in St. Louis, USA) [21]. MHV A59-GFP and VSV-SARS-CoV-2 were propagated as
101 described [20,21].

102

103 **Infectivity assays**

104 Huh7 cells (1.6×10^6 cells/well in 6-well plates) were infected with approximately 100 PFU of
105 HCoV-229E pre-exposed for 10 min at 37°C to EGCG or dimethyl sulfoxide (DMSO) vehicle in
106 DMEM. Inocula were removed 2 h later, and monolayers were overlaid with 1.2%
107 carboxymethylcellulose in DMEM containing 2% FBS. Infected cells were incubated at 33°C in
108 5% CO_2 until 4 days post-infection, when they were fixed with 10% formalin and stained with 1%
109 (wt/vol) crystal violet–10% (vol/vol) ethanol in H_2O for counting plaques.

110 Huh7 and A549 cells (4×10^5 cells/well in 24-well plates) were infected with
111 approximately 200 focus-forming units (FFU) of HCoV-OC43, pre-exposed to EGCG or DMSO
112 vehicle for 10 min at 37°C in DMEM. Inocula were removed 2 h later, and monolayers were
113 overlaid with 1.2% microcrystalline colloidal cellulose (Sigma-Aldrich 435244) in DMEM
114 containing 2% FBS. Infected cells were incubated at 33°C in 5% CO_2 for 3 days, then fixed and

115 processed for immunofluorescence to detect OC43 nucleoprotein. Cells were incubated with
116 primary mouse IgG anti-coronavirus group antibody MAB9013 (Millipore Sigma; diluted 1:500)
117 for 1 h at room temperature, followed by addition of secondary Alexa Fluor 488 anti-mouse IgG
118 Fab 2 antibody (Cell Signaling Technology 4408S) for 1 h at room temperature. Foci were
119 visualized and counted under a fluorescence microscope (Nikon Eclipse Ts2).

120 MHV A59-GFP virions pre-exposed to EGCG or the DMSO vehicle control for 10 min at
121 37°C in DMEM were used to infect L929 cell monolayers. Inocula were removed 1 h later, and
122 monolayers were overlaid with 1.2% carboxymethylcellulose in DMEM containing 2% FBS.
123 Infected cells were incubated at 33°C in 5% CO_2 for 24 h, then fixed prior to counting of GFP-
124 positive cells under the fluorescence microscope.

125 VSV-SARS-CoV-2 S virions pre-exposed to EGCG or the DMSO vehicle control for 10
126 min at 37°C in DMEM were used to infect Huh7, A549-ACE2 or Calu-3 cell monolayers in
127 duplicate wells of a 96-well plate. Infected cells were incubated at 33°C in 5% CO_2 for 24 h, then
128 fixed with 10% formalin. GFP signals were captured by Nikon Eclipse Ts2, processed using the
129 Python Imaging Library to find the mean grey value, and plotted as percentage of inhibition.

130 In all experiments, half maximal inhibitory concentrations (IC_{50}) were calculated by
131 nonlinear regression analysis using GraphPad Prism (version 9.0; GraphPad Software, Inc.).

132

133 **Pseudoparticle entry assays**

134 Lentiviral pseudoparticles were generated in HEK293T/17 cells by co-transfection using
135 Lipofectamine 2000 (Invitrogen 11668-019) [22]. The CoV spike expression plasmids were co-
136 transfected with a luciferase-encoding lentiviral genome, and plasmids encoding HIV-1 gag/pol,
137 tat, and rev [22]. Cell culture supernatants containing coronavirus spike pseudotyped lentiviral

138 particles were collected at 48 and 72 hours post-transfection, pooled and filtered through a 0.45
139 μm filter, and stored at -80°C.
140 Pseudoparticles were incubated for 10 min at 37°C with serially diluted EGCG and used
141 to infect Huh7 or A549-ACE2 cells in triplicate in 96-well plates. Infectivity was determined after
142 3 days by luminescence following addition of BrightGlo reagent (Promega PR-E2620). IC_{50} were
143 calculated by nonlinear regression analysis using GraphPad Prism (version 9.0; GraphPad
144 Software, Inc.).
145
146 **Cell toxicity assay**
147 Cells (50,000 per well in 96-well plate) were treated with EGCG or DMSO in DMEM and
148 incubated at 37°C in 5% CO_2 for 2h. To mimic the conditions used in the infectivity and
149 pseudoparticle assays, media was removed, cells were washed with PBS, and supplemented with
150 normal culture media of DMEM with 10% FBS, 50 U/mL penicillin, and 50 μg/mL streptomycin.
151 After 72 h, cell viability was assessed by alamarBlue cell viability reagent (Invitrogen DAL1025)
152 on a fluorescence plate reader (SpectraMax ID3 Multimode Plate reader).
153
154 **Time-of-addition experiments**
155 Near-confluent Huh7 and A549 cell monolayers in 12 or 24-well plates were pre-treated with
156 EGCG or DMSO vehicle for 1 h at 37°C in DMEM. Cells were washed with DMEM and infected
157 with 50-200 PFU of HCoV-229E or HCoV-OC43 for 2 h at 33°C. Alternatively, Huh7 and A549
158 cells were first infected with HCoV-229E or HCoV-OC43 for 2 h at 33°C. After removing the
159 inocula, the infected cells were overlaid with 1.2% microcrystalline colloidal cellulose in DMEM-

160 2% FBS containing EGCG or DMSO. Infectivity was assessed by plaquing efficiency or
161 immunostaining.
162
163 **Binding assays**
164 OC43 (4 x 10^4 PFU; MOI 0.05) or VSV-SARS-CoV-2 (2 x 10^5 PFU; MOI 0.5, chosen to match
165 the conditions of the infectivity assay) were exposed for 10 min at 37°C to EGCG or DMSO in
166 DMEM and adsorbed onto pre-chilled Huh7 and A549 cells for 1 h at 4°C. After three washes
167 with cold phosphate-buffered saline (PBS), cells were lysed and RNA was isolated using the
168 Monarch Total RNA Miniprep Kit (NEB T2010S), according to the manufacturer's instructions.
169 The RNA was transcribed to cDNA using the High Capacity cDNA Reverse Transcription Kit
170 (Applied Biosystems LS4368814). Quantitative real-time PCR was performed on the QuantStudio
171 3 (Applied Biosystems) instrument, using PowerTrack SYBR Green Master Mix (Applied
172 Biosystems LSA46110), with primers to detect actin (F: 5'-CTGGGAGTGGGTGGAGGC-3', R:
173 5'-TCAACTGGTCTCAAGTCAGTG-3') and OC43 N gene (F: 5'-
174 CCCAAGCAAACTGCTACCTCTCAG-3', R: 5'-GTAGACTCCGTCAATATCGGTGCC-3')
175 or VSV N gene (F: 5'-GATAGTACCGGAGGATTGACGACTA-3', R: 5'-
176 TCAAACCATCCGAGCCATTC-3'). Following normalization to actin, the percentage of binding
177 was expressed relative to binding of virions treated with the DMSO control.
178
179 **Results**
180 **EGCG inhibits murine and human coronavirus infection.**
181 We first tested the effect of EGCG on the infectivity of human common cold coronaviruses HCoV-
182 229E (an alphacoronavirus) and HCoV-OC43 (a betacoronavirus). HCoV-229E and HCoV-OC43

183 virions were treated with DMSO or varying concentrations of EGCG for 10 min at 37°C and used
184 to inoculate infection-susceptible human hepatoma Huh7 or human lung epithelial A549 cell
185 monolayers. After 2 h of infection, inocula were removed and cells were overlaid with plaquing
186 media. Infectivity was assessed by plaquing efficiency on Huh7 for HCoV-229E or by
187 immunofluorescence focus-forming assay on Huh7 and A549 cells for HCoV-OC43. EGCG
188 inhibited infectivity of HCoV-229E (IC_{50} = 0.77 μM) and HCoV-OC43 (IC_{50} = 0.49-0.56 μM) at
189 sub- to low micromolar concentrations (**Figure 1A**), similar to other viruses highly susceptible to
190 inhibition by EGCG, such as HSV-1 [19]. We next tested the inhibitory activity of EGCG against
191 a murine CoV, murine hepatitis virus (MHV-A59), on murine fibroblast L929 cell monolayers.
192 We observed that EGCG inhibited MHV-A59 infection with similar potency as for the human
193 common cold CoVs (IC_{50} = 0.71 μM) (**Figure 1B**) and inhibited the formation of syncytia (**Figure**
194 **1C**). Consistent with previous reports, we found EGCG to have minimal effect on cell viability at
195 the low micromolar range in which antiviral activity is exerted (**Figure 1D**).
196
197 **Entry of highly pathogenic coronaviruses is blocked by EGCG.**
198 We produced luciferase-encoding lentiviral particles pseudotyped with SARS-CoV-1, SARS-
199 CoV-2 and MERS-CoV spike (S) proteins to investigate the effect of EGCG on entry of highly
200 pathogenic coronaviruses. We also generated lentiviral particles pseudotyped with the spike
201 protein of WIV1-CoV, a bat coronavirus that binds to human ACE2 [23]. Huh7 cells were
202 inoculated with CoV S pseudoparticles pre-exposed to EGCG or DMSO for 10 min at 37°C.
203 Inocula were removed after 2 h and replaced with fresh DMEM. After 72 h, cells were lysed and
204 luminescence was measured. EGCG inhibited SARS-CoV-1, SARS-CoV-2, MERS-CoV and
205 WIV1-CoV pseudoparticle entry with IC_{50} of 2.5, 48.6, 13.7 and 3.8 μM, respectively (**Figure**

206 **2A**). To evaluate the antiviral effect in a more relevant cell type, we generated A549 cells stably
207 expressing human ACE2, the receptor for SARS-CoV-1 and SARS-CoV-2, and isolated a clone
208 with high levels of ACE2 expression and enhanced susceptibility to SARS-CoV-2 S
209 pseudoparticle infection (**Supplemental Figure 1**). We found that EGCG also inhibited entry of
210 SARS-CoV-1, SARS-CoV-2, and WIV1-CoV pseudoparticles into A549-ACE2 B9 cells, with
211 IC_{50} of 15.9, 24.0 and 24.5 μM, respectively (**Figure 2A**).
212

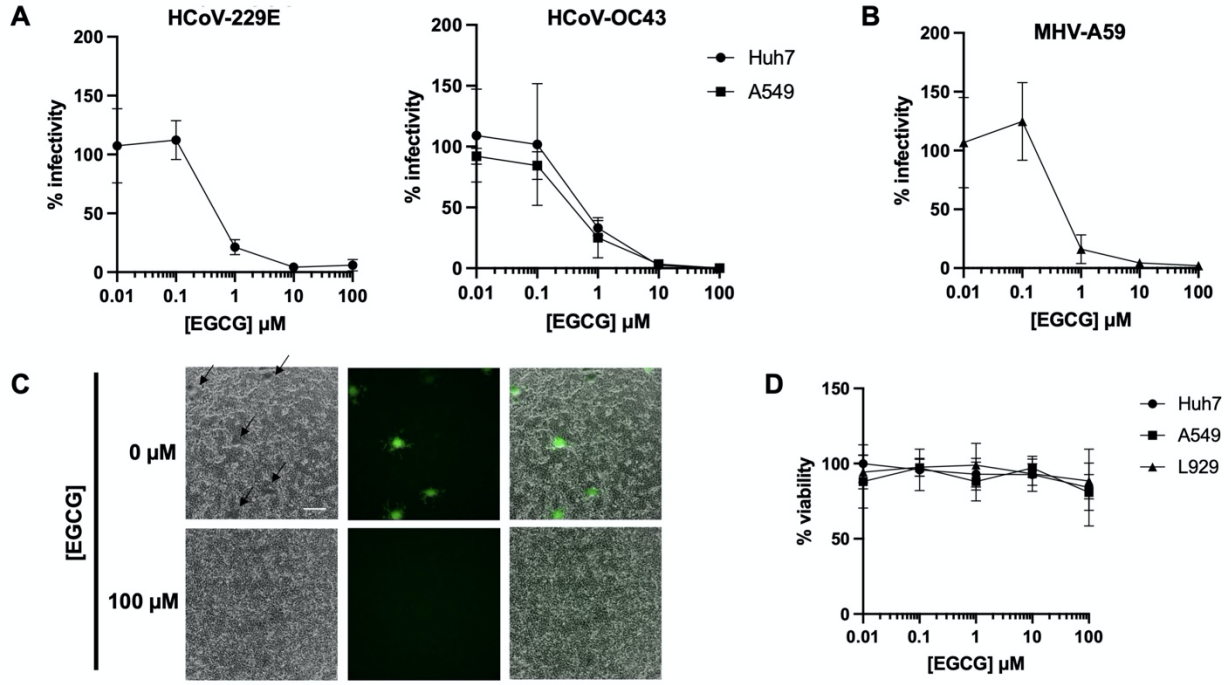

213

214 **Figure 1. EGCG pre-treatment inhibits diverse CoV infections.** Pre-treatment of authentic
215 HCoV-229E and HCoV-OC43 **(A)** or murine coronavirus MHV-A59 **(B)** with EGCG for 10 min
216 at 37°C prevented infection of Huh7, A549 or L292 cells, respectively. Mean values with standard
217 deviation of three independent experiments are plotted. **(C)** A reduction in syncytia (black arrows)
218 was observed for EGCG-treated MHV-A59. Scale bar: 200 μm. **(D)** Cell exposure to EGCG during
219 the 2 h infection had minimal effect on cell viability. Mean values with standard deviation of two
220 independent experiments with duplicates are plotted.
221

222 We next assessed the effect of EGCG on replication-competent vesicular stomatitis virus
223 (VSV) virions expressing GFP and SARS-CoV-2 S instead of the VSV glycoprotein (VSV-SARS-

224 CoV-2) [21]. Huh7, A549-ACE2, and lung epithelial Calu-3 cells were infected with EGCG-
225 treated VSV-SARS-CoV-2 virions (MOI of 5). Infected cells were imaged by fluorescence
226 microscopy after 24 h. Similar to the pseudoparticle assays, EGCG inhibited VSV-SARS-CoV-2
227 S infection with IC_{50} ranging from 11.45 to 15.40 μM, depending on the cell type (**Figure 2B**),
228 with minimal cytotoxicity up to 100 μM (**Supplemental Figure 2**). We next evaluated whether
229 the effect of EGCG was dependent on MOI. Using the same assay, but with MOI of 0.5, we found
230 that EGCG inhibited VSV-SARS-CoV-2 infection with IC_{50} ranging from 0.14 to 1.13 μM. These
231 findings demonstrate that the inhibitory activity of EGCG depends on the MOI (**Figure 2B**),
232 consistent with the virions as the proposed target of EGCG [19]. This also provides a potential
233 explanation for the difference in IC_{50} for authentic viruses investigated at low MOI (<0.001)
234 (**Figure 1A-B**) compared to lentiviral pseudoparticles (**Figure 2A**), for which p24 ELISA data for
235 lentiviral particles pseudotyped with SARS-CoV-2 spike in our laboratory provide an estimate of
236 approximately 1.7 x 10^6 transducing units per mL, resulting in an apparent MOI of 3.4.
237
238 **EGCG acts on virions to inhibit coronavirus binding to cell surfaces.**
239 To confirm that EGCG acts on CoV virions, and not on cells, we performed time-of-addition
240 experiments. Cells were pre-treated with EGCG or DMSO 1 h at 37°C, at which point media was
241 removed and cells were infected with HCoV-229E or HCoV-OC43. Infectivity was determined by
242 plaque assay or immunostaining. Alternatively, cells were infected, and EGCG- or DMSO-
243 containing medium was added 2 h post-infection. In either condition, no inhibition of infectivity
244 was observed until the highest concentration of 100 μM EGCG (**Figure 3A**). To test if EGCG
245 inhibits CoV attachment, we performed binding assays in which cells were incubated with pre-
246 treated virions at 4°C for 1 h to allow for attachment, but not fusion or entry. After cell washing,

247 bound virions were quantified by RT-qPCR (**Supplemental Figure 3**). Pre-chilled Huh7 or Calu-
248 3 cells were inoculated with HCoV-OC43 or VSV-SARS-CoV-2 treated with DMSO, 10 μM
249 EGCG, or 20 μg/mL heparin, as a control attachment inhibitor [11]. As expected, heparin partially
250 blocked VSV-SARS-CoV-2 binding. We also observed that heparin reduced HCoV-OC43
251 binding, which unlike other coronavirus does not have a known protein receptor but depends on
252 sialic acid, and, as recently reported, glycosaminoglycans for entry [24]. EGCG similarly reduced
253 VSV-SARS-CoV-2 binding to Huh7 and Calu-3 cells (**Figure 3B-C**).
254

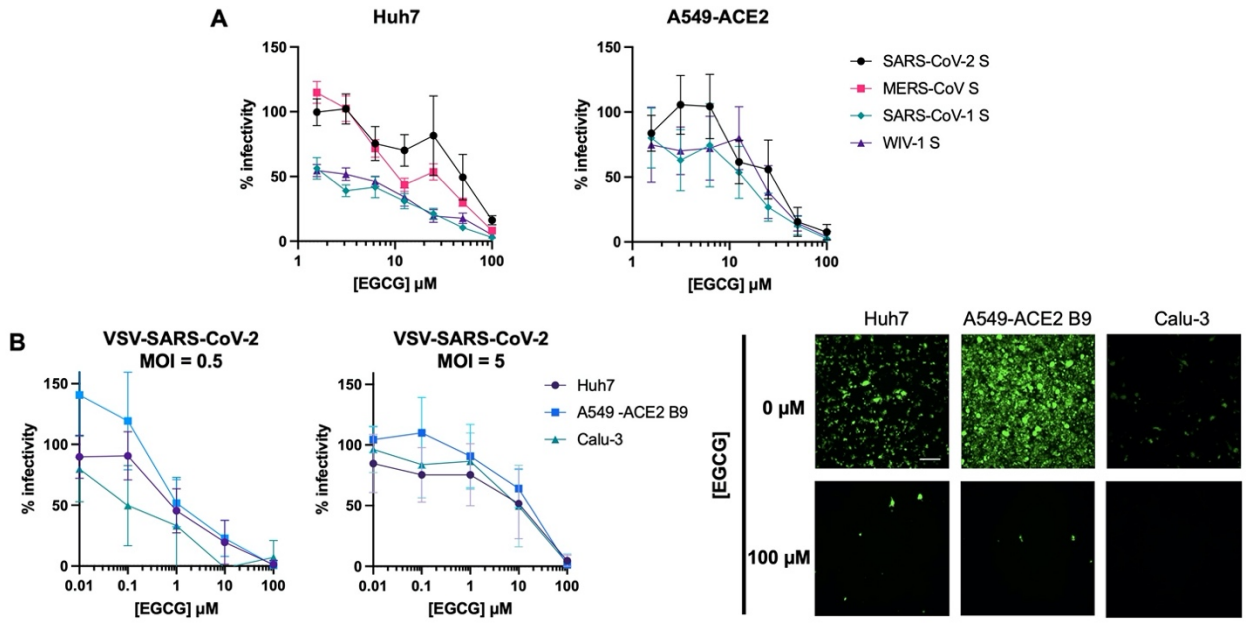

255

256 **Figure 2. EGCG inhibits entry of highly pathogenic CoVs. (A)** EGCG treatment reduced entry
257 of lentiviral particles pseudotyped with S from SARS-CoV-1, MERS-CoV, SARS-CoV-2, or
258 WIV1-CoV. Mean values with standard error of the mean of three independent experiments each
259 done in triplicates are plotted. **(B)** EGCG displayed MOI-dependent inhibition of VSV-SARS-
260 CoV-2 in Huh7, A549-ACE2 B9 and Calu-3. Mean values with standard deviation of three
261 independent experiments each in duplicates are plotted. Representative images are shown. Scale
262 bar: 200 μm.
263

264

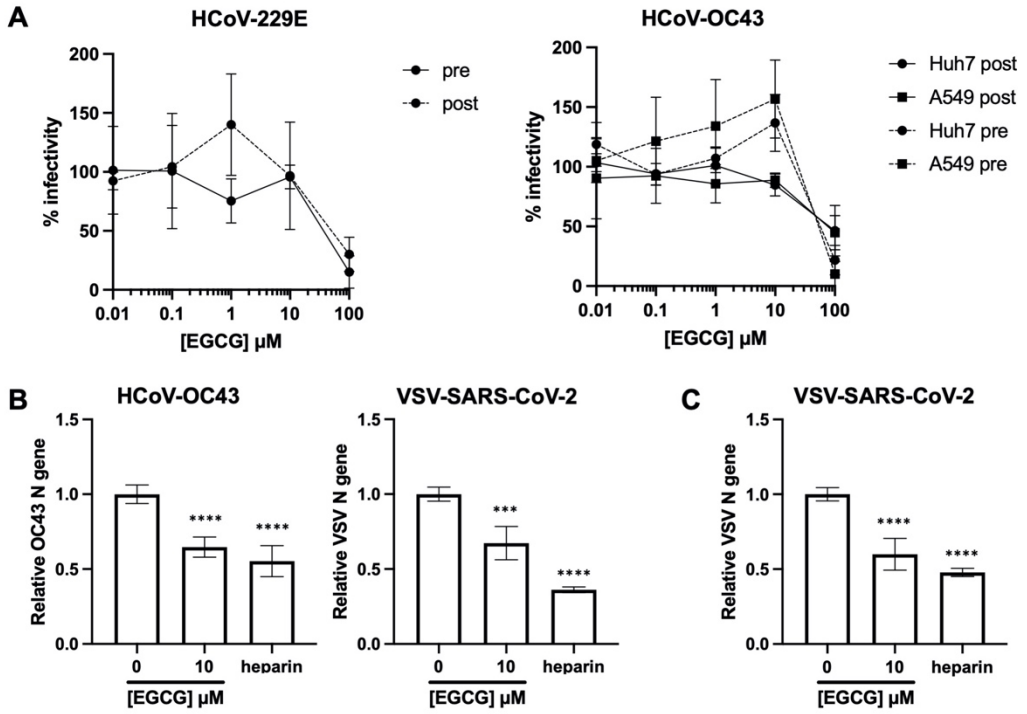

Figure 3. EGCG inhibits CoV attachment to cells. (A) Cell pre-treatment or post-229E and OC43 infection treatment does not restrict infection to similar extents as virion pre-treatment. Mean values with standard deviation of three independent experiments are plotted. (B) Virions were pre-treated with EGCG or heparin for 10 min at 37°C then cooled on ice and added to pre-chilled Huh7 (B) or Calu-3 cells (C) for 1 hour on ice. Attached virus was quantified by RT-qPCR after washing cells with PBS three times. Mean values with standard deviation from qPCR triplicates of two independent experiments are plotted.

Discussion

Green tea catechins, especially EGCG, exert antiviral effects against diverse viruses. We show that EGCG broadly inhibits CoV infections, and that its activity is due, at least in part, to blocking CoV attachment to target cells. Infection by authentic murine and human CoVs, as well as entry of lentivirus particles pseudotyped with spike proteins of highly pathogenic or potentially emerging CoVs [23], was inhibited by EGCG treatment. Interestingly, EGCG was recently shown to significantly inhibit authentic SARS-CoV-2 infection, and time-of-addition experiments suggested that EGCG at least partially blocks SARS-CoV-2 entry [25], consistent with our findings. In this

283 study, we expand the scope of EGCG activity to other CoVs, including murine and bat CoVs, and
284 demonstrate the physiological relevance of the inhibitory activity of EGCG on CoV attachment
285 and infection of lung epithelial cells.

286 A variety of mechanisms for the antiviral activity of EGCG have previously been
287 described. EGCG inhibits the primary attachment of diverse viruses including VSV, IAV, HCV,
288 HSV-1 and vaccinia virus [19]. EGCG is proposed to act directly on HCV virions to block
289 attachment in a genotype independent manner, with no alteration in HCV (co)-receptor expression
290 nor any effect on viral replication, assembly, or release [26,27]. As for HBV, EGCG may inhibit
291 entry [28], as well as replication, with proposed roles in impairing HBV replicative intermediates
292 during DNA synthesis [29], diminishing the transcriptional activation of the HBV core promoter
293 [30], and enhancing lysosomal acidification to adversely affect HBV replication [31].
294 Alternatively, EGCG is suggested to prevent the binding of HIV glycoprotein 120 to its receptor
295 molecule CD4 on cells [32], and to act as an HIV reverse transcriptase inhibitor [33]. Finally,
296 recent studies have identified *in vitro* inhibitory effects of EGCG against the SARS-CoV-2 3C-
297 like protease [34–37]. However, our time-of-addition experiments with HCoV-229E and HCoV-
298 OC43, as well as those of others with SARS-CoV-2 [25], strongly suggest that EGCG
299 predominantly inhibits authentic CoV infection by blocking entry, although other activities might
300 be exerted at higher concentrations. Furthermore, we show that EGCG reduces cell surface binding
301 of HCoV-OC43 and VSV-SARS-CoV-2, in a similar manner to heparin, which has been
302 demonstrated to competitively block virion attachment [11].

303 While COVID-19 vaccine development and deployment are ongoing, extensive efforts are
304 underway to identify antibodies, peptides, and small molecules to prevent SARS-CoV-2 entry [38].
305 To protect against emerging CoVs, the identification of broad-spectrum entry inhibitors is a

306 priority. Recently, lactoferrins have been described to disrupt CoV primary attachment, mediated
307 by heparan sulfate interactions, conferring antiviral activity against multiple CoVs *in vitro*,
308 demonstrating the potential for a pan-coronavirus inhibitor [39]. Small molecules continue to be
309 preferred as drugs in general due to superior pharmacokinetic properties and simpler synthesis
310 [40]. As with other green tea catechins, EGCG does not accumulate at high levels, is unstable
311 under physiological conditions, and is rapidly metabolized [41–43]. However, the observation that
312 a small molecule exerts pan-coronavirus activity provides the basis for the development of entry
313 inhibitors that could provide an effective antiviral strategy to protect against future emerging CoV
314 infections.
315

316 **Funding information**

317 This work was supported by a Natural Sciences and Engineering Research Council of Canada
318 Discovery Grant, a Banting Research Foundation Discovery Award, as well as by the Canadian
319 Foundation for Innovation John R. Evans Leaders Fund, and Queen's University. E.V.L. is
320 supported by a Vanier Canada Graduate Scholarship.
321

322 **Acknowledgements**

323 The following reagents were obtained through BEI Resources (NIAID, NIH): *Homo sapiens* A549
324 Lung Carcinoma Cells (NR-52268); Murine 17CL1 Cell Line (NR-53719); SARS-Related
325 Coronavirus 2, Wuhan-Hu-1Spike-Pseudotyped Lentiviral Kit (NR-52948); Human Coronavirus
326 OC43 (NR-52725) and 229E (NR-52726). We thank Gerard O'Leary for Python processing scripts,
327 Dr. Selena Sagan (McGill University) for providing coronavirus infection protocols, and Dr.
328 Chantelle Capicciotti (Queen's University) for helpful discussions.

329 **References**

330 1. Li, W.; Shi, Z.; Yu, M.; Ren, W.; Smith, C.; Epstein, J.H.; Wang, H.; Crameri, G.; Hu, Z.;
331 Zhang, H.; et al. Bats Are Natural Reservoirs of SARS-Like Coronaviruses. *Science.*
332 **2005**, *310*, 676–679, doi:10.1126/science.1118391.
333 2. Walsh, E.E.; Shin, J.H.; Falsey, A.R. Clinical impact of human coronaviruses 229E and
334 OC43 infection in diverse adult populations. *J. Infect. Dis.* **2013**, *208*, 1634–1642,
335 doi:10.1093/infdis/jit393.
336 3. Patrick, D.M.; Petric, M.; Skowronski, D.M.; Guasparini, R.; Booth, T.F.; Krajden, M.;
337 McGeer, P.; Bastien, N.; Gustafson, L.; Dubord, J.; et al. An Outbreak of Human
338 Coronavirus OC43 Infection and Serological Cross-reactivity with SARS Coronavirus.
339 *Can. J. Infect. Dis. Med. Microbiol.* **2006**, *17*, 330–336, doi:10.1155/2006/152612.
340 4. Hand, J.; Rose, E.B.; Salinas, A.; Lu, X.; Sakthivel, S.K.; Schneider, E.; Watson, J.T.
341 Severe respiratory illness outbreak associated with human coronavirus NL63 in a long-
342 term care facility. *Emerg. Infect. Dis.* **2018**, *24*, 1964–1966, doi: 10.3201/eid2410.180862.
343 5. Milewska, A.; Zarebski, M.; Nowak, P.; Stozek, K.; Potempa, J.; Pyrc, K. Human
344 coronavirus NL63 utilizes heparan sulfate proteoglycans for attachment to target cells. *J.*
345 *Virol.* **2014**, *88*, 13221–13230, doi:10.1128/JVI.02078-14.
346 6. WuDunn, D.; Spear, P.G. Initial interaction of herpes simplex virus with cells is binding
347 to heparan sulfate. *J. Virol.* **1989**, *63*, 52–58, doi:10.1128/JVI.63.1.52-58.1989.
348 7. Lycke, E.; Johansson, M.; Svennerholm, B.; Lindahl, U. Binding of herpes simplex virus
349 to cellular heparan sulphate, an initial step in the adsorption process. *J. Gen. Virol.* **1991**,
350 *72*, 1131–1137, doi:10.1099/0022-1317-72-5-1131.
351 8. Germi, R.; Crance, J.-M.; Garin, D.; Guimet, J.; Lortat-Jacob, H.; Ruigrok, R.W.H.;

352 Zarski, J.-P.; Drouet, E. Cellular glycosaminoglycans and low density lipoprotein receptor
353 are involved in hepatitis C virus adsorption. *J. Med. Virol.* **2002**, *68*, 206–215,
354 doi:10.1002/jmv.10196.
355 9. Morikawa, K.; Zhao, Z.; Date, T.; Miyamoto, M.; Murayama, A.; Akazawa, D.; Tanabe,
356 J.; Sone, S.; Wakita, T. The roles of CD81 and glycosaminoglycans in the adsorption and
357 uptake of infectious HCV particles. *J. Med. Virol.* **2007**, *79*, 714–723,
358 doi:10.1002/jmv.20842.
359 10. Patel, M.; Yanagishita, M.; Roderiquez, G.; Bou-Habib, D.C.; Oravecz, T.; Hascall, V.C.;
360 Norcorss, M.A. Cell-Surface Heparan Sulfate Proteoglycan Mediates HIV-1 Infection of
361 T-Cell Lines. *AIDS Res. Hum. Retroviruses* **1993**, *9*, 167–174,
362 doi:10.1089/aid.1993.9.167.
363 11. Clausen, T.M.; Sandoval, D.R.; Spliid, C.B.; Pihl, J.; Perrett, H.R.; Painter, C.D.;
364 Narayanan, A.; Majowicz, S.A.; Kwong, E.M.; McVicar, R.N.; et al. SARS-CoV-2
365 Infection Depends on Cellular Heparan Sulfate and ACE2. *Cell* **2020**, *183*, 1043-
366 1057.e15, doi:10.1016/j.cell.2020.09.033.
367 12. Zhang, Q.; Chen, C.Z.; Swaroop, M.; Xu, M.; Wang, L.; Lee, J.; Wang, A.Q.; Pradhan,
368 M.; Hagen, N.; Chen, L.; et al. Heparan sulfate assists SARS-CoV-2 in cell entry and can
369 be targeted by approved drugs in vitro. *Cell Discov.* **2020**, *6*, 80, doi:10.1038/s41421-020-
370 00222-5.
371 13. Krempl, C.; Schultze, B.; Herrler, G. Analysis of cellular receptors for human coronavirus
372 OC43. *Adv Exp Med Bio*. **1995**, 380, 371–4, doi:10.1007/978-1-4615-1899-0_60.
373 14. Huang, X.; Dong, W.; Milewska, A.; Golda, A.; Qi, Y.; Zhu, Q.K.; Marasco, W.A.; Baric,
374 R.S.; Sims, A.C.; Pyrc, K.; et al. Human Coronavirus HKU1 Spike Protein Uses O -

375 Acetylated Sialic Acid as an Attachment Receptor Determinant and Employs
376 Hemagglutinin-Esterase Protein as a Receptor-Destroying Enzyme. *J. Virol.* **2015**, *89*,
377 7202–13, doi:10.1128/jvi.00854-15.
378 15. Weis, W.; Brown, J.H.; Cusack, S.; Paulson, J.C.; Skehel, J.J.; Wiley, D.C. Structure of
379 the influenza virus haemagglutinin complexed with its receptor, sialic acid. *Nature* **1988**,
380 *333*, 426–431, doi:10.1038/333426a0.
381 16. Hofmann, H.; Pyrc, K.; van der Hoek, L.; Geier, M.; Berkhout, B.; Pöhlmann, S. Human
382 coronavirus NL63 employs the severe acute respiratory syndrome coronavirus receptor for
383 cellular entry. *Proc. Natl. Acad. Sci.* **2005**, *102*, 7988–7993,
384 doi:10.1073/pnas.0409465102.
385 17. Hoffmann, M.; Kleine-Weber, H.; Schroeder, S.; Krüger, N.; Herrler, T.; Erichsen, S.;
386 Schiergens, T.S.; Herrler, G.; Wu, N.-H.; Nitsche, A.; et al. SARS-CoV-2 Cell Entry
387 Depends on ACE2 and TMPRSS2 and Is Blocked by a Clinically Proven Protease
388 Inhibitor. *Cell* **2020**, *181*, 271-280.e8, doi:10.1016/j.cell.2020.02.052.
389 18. Xu, J.; Xu, Z.; Zheng, W. A Review of the Antiviral Role of Green Tea Catechins.
390 *Molecules* **2017**, *22*, 1337, doi:10.3390/molecules22081337.
391 19. Colpitts, C.C.; Schang, L.M. A Small Molecule Inhibits Virion Attachment to Heparan
392 Sulfate- or Sialic Acid-Containing Glycans. *J. Virol.* **2014**, *88*, 7806–7817,
393 doi:10.1128/JVI.00896-14.
394 20. Coley, S.E.; Lavi, E.; Sawicki, S.G.; Fu, L.; Schelle, B.; Karl, N.; Siddell, S.G.; Thiel, V.
395 Recombinant mouse hepatitis virus strain A59 from cloned, full-length cDNA replicates to
396 high titers in vitro and is fully pathogenic in vivo. *J. Virol.* **2005**, *79*, 3097–3106,
397 doi:10.1128/JVI.79.5.3097-3106.2005.

398 21. Case, J.B.; Rothlauf, P.W.; Chen, R.E.; Liu, Z.; Zhao, H.; Kim, A.S.; Bloyet, L.-M.; Zeng,
399 Q.; Tahan, S.; Droit, L.; et al. Neutralizing Antibody and Soluble ACE2 Inhibition of a
400 Replication-Competent VSV-SARS-CoV-2 and a Clinical Isolate of SARS-CoV-2. *Cell*
401 *Host Microbe* **2020**, *28*, 475-485.e5, doi:10.1016/j.chom.2020.06.021.
402 22. Crawford, K.H.D.; Eguia, R.; Dingens, A.S.; Loes, A.N.; Malone, K.D.; Wolf, C.R.; Chu,
403 H.Y.; Tortorici, M.A.; Veesler, D.; Murphy, M.; et al. Protocol and Reagents for
404 Pseudotyping Lentiviral Particles with SARS-CoV-2 Spike Protein for Neutralization
405 Assays. *Viruses.* **2020**, *12*, 513, doi:10.1007/978-1-4615-1899-0_60.
406 23. Ge, X.-Y.; Li, J.-L.; Yang, X.-L.; Chmura, A.A.; Zhu, G.; Epstein, J.H.; Mazet, J.K.; Hu,
407 B.; Zhang, W.; Peng, C.; et al. Isolation and characterization of a bat SARS-like
408 coronavirus that uses the ACE2 receptor. *Nature* **2013**, *503*, 535–538,
409 doi:10.1038/nature12711.
410 24. Wang, R.; Simoneau, C.R.; Kulsuptrakul, J.; Bouhaddou, M.; Travisano, K.A.; Hayashi,
411 J.M.; Carlson-Stevermer, J.; Zengel, J.R.; Richards, C.M.; Fozouni, P.; et al. Genetic
412 Screens Identify Host Factors for SARS-CoV-2 and Common Cold Coronaviruses. *Cell*
413 **2021**, *184*, 106-119.e14, doi:10.1016/j.cell.2020.12.004.
414 25. Henss, L.; Auste, A.; Schürmann, C.; Schmidt, C.; von Rhein, C.; Mühlebach, M.D.;
415 Schnierle, B.S. The green tea catechin epigallocatechin gallate inhibits SARS-CoV-2
416 infection. *J. Gen. Virol.* **2021**, *102*, doi:10.1099/jgv.0.001574.
417 26. Calland, N.; Albecka, A.; Belouzard, S.; Wychowski, C.; Duverlie, G.; Descamps, V.;
418 Hober, D.; Dubuisson, J.; Rouillé, Y.; Séron, K. (−)-Epigallocatechin-3-gallate is a new
419 inhibitor of hepatitis C virus entry. *Hepatology* **2012**, *55*, 720–729,
420 doi:10.1002/hep.24803.

421 27. Ciesek, S.; von Hahn, T.; Colpitts, C.C.; Schang, L.M.; Friesland, M.; Steinmann, J.;
422 Manns, M.P.; Ott, M.; Wedemeyer, H.; Meuleman, P.; et al. The green tea polyphenol,
423 epigallocatechin-3-gallate, inhibits hepatitis C virus entry. *Hepatology* **2011**, *54*, 1947–
424 1955, doi:10.1002/hep.24610.
425 28. Huang, H.-C.; Tao, M.-H.; Hung, T.-M.; Chen, J.-C.; Lin, Z.-J.; Huang, C. (−)-
426 Epigallocatechin-3-gallate inhibits entry of hepatitis B virus into hepatocytes. *Antiviral*
427 *Res.* **2014**, *111*, 100–111, doi:10.1016/j.antiviral.2014.09.009.
428 29. He, W.; Li, L.X.; Liao, Q.J.; Liu, C.L.; Chen, X.L. Epigallocatechin gallate inhibits HBV
429 DNA synthesis in a viral replication - inducible cell line. *World J. Gastroenterol.* **2011**,
430 *17*, 1507–1514, doi:10.3748/wjg.v17.i11.1507.
431 30. Xu, J.; Gu, W.; Li, C.; Li, X.; Xing, G.; Li, Y.; Song, Y.; Zheng, W. Epigallocatechin
432 gallate inhibits hepatitis B virus via farnesoid X receptor alpha. *J. Nat. Med.* **2016**, *70*,
433 584–591, doi:10.1007/s11418-016-0980-6.
434 31. Zhong, L.; Hu, J.; Shu, W.; Gao, B.; Xiong, S. Epigallocatechin-3-gallate opposes HBV-
435 induced incomplete autophagy by enhancing lysosomal acidification, which is unfavorable
436 for HBV replication. *Cell Death Dis.* **2015**, *6*, e1770–e1770, doi:10.1038/cddis.2015.136.
437 32. Williamson, M.P.; McCormick, T.G.; Nance, C.L.; Shearer, W.T. Epigallocatechin
438 gallate, the main polyphenol in green tea, binds to the T-cell receptor, CD4: Potential for
439 HIV-1 therapy. *J. Allergy Clin. Immunol.* **2006**, *118*, 1369–1374,
440 doi:10.1016/j.jaci.2006.08.016.
441 33. Li, S.; Hattori, T.; Kodama, E.N. Epigallocatechin gallate inhibits the HIV reverse
442 transcription step. *Antivir. Chem. Chemother.* **2011**, *21*, 239–243, doi:10.3851/IMP1774.
443 34. Jang, M.; Park, R.; Park, Y.-I.; Cha, Y.-E.; Yamamoto, A.; Lee, J.I.; Park, J. EGCG, a

green tea polyphenol, inhibits human coronavirus replication in vitro. *Biochem. Biophys. Res. Commun.* **2021**, *547*, 23–28, doi:10.1016/j.bbrc.2021.02.016.

35. Jang, M.; Park, Y.-I.; Cha, Y.-E.; Park, R.; Namkoong, S.; Lee, J.I.; Park, J. Tea Polyphenols EGCG and Theaflavin Inhibit the Activity of SARS-CoV-2 3CL-Protease *In Vitro*. *Evidence-Based Complement. Altern. Med.* **2020**, *2020*, 5630838, doi:10.1155/2020/5630838.

36. Chiou, W.-C.; Chen, J.-C.; Chen, Y.-T.; Yang, J.-M.; Hwang, L.-H.; Lyu, Y.-S.; Yang, H.-Y.; Huang, C. The inhibitory effects of PGG and EGCG against the SARS-CoV-2 3C-like protease. *Biochem. Biophys. Res. Commun.* **2021**, *S0006-291X*, 32299–3, doi:10.1016/j.bbrc.2020.12.106.

37. Du, A.; Zheng, R.; Disoma, C.; Li, S.; Chen, Z.; Li, S.; Liu, P.; Zhou, Y.; Shen, Y.; Liu, S.; et al. Epigallocatechin-3-gallate, an active ingredient of Traditional Chinese Medicines, inhibits the 3CLpro activity of SARS-CoV-2. *Int. J. Biol. Macromol.* **2021**, *176*, 1–12, doi:10.1016/j.ijbiomac.2021.02.012.

38. Xiu, S.; Dick, A.; Ju, H.; Mirzaie, S.; Abdi, F.; Cocklin, S.; Zhan, P.; Liu, X. Inhibitors of SARS-CoV-2 Entry: Current and Future Opportunities. *J. Med. Chem.* **2020**, *63*, 12256–12274, doi:10.1021/acs.jmedchem.0c00502.

39. Hu, Y.; Meng, X.; Zhang, F.; Xiang, Y.; Wang, J. The in vitro antiviral activity of lactoferrin against common human coronaviruses and SARS-CoV-2 is mediated by targeting the heparan sulfate co-receptor. *Emerg. Microbes Infect.* **2021**, *10*, 317–330, doi:10.1080/22221751.2021.1888660.

40. Ngo, H.X.; Garneau-Tsodikova, S. What are the drugs of the future? *Medchemcomm* **2018**, *9*, 757–758, doi:10.1039/c8md90019a.

467 41. Lambert, J.D.; Lee, M.-J.; Lu, H.; Meng, X.; Hong, J.J.J.; Seril, D.N.; Sturgill, M.G.;
468 Yang, C.S. Epigallocatechin-3-Gallate Is Absorbed but Extensively Glucuronidated
469 Following Oral Administration to Mice. *J. Nutr.* **2003**, *133*, 4172–4177,
470 doi:10.1093/jn/133.12.4172.
471 42. Chow, H.-H.S.; Cai, Y.; Hakim, I.A.; Crowell, J.A.; Shahi, F.; Brooks, C.A.; Dorr, R.T.;
472 Hara, Y.; Alberts, D.S. Pharmacokinetics and Safety of Green Tea Polyphenols after
473 Multiple-Dose Administration of Epigallocatechin Gallate and Polyphenon E in Healthy
474 Individuals. *Clin. Cancer Res.* **2003**, *9*, 3312–3319.
475 43. Smith, T.J. Green tea polyphenols in drug discovery: a success or failure? *Expert Opin.*
476 *Drug Discov.* **2011**, *6*, 589–595, doi:10.1517/17460441.2011.570750.
477
478